

Occlusion of Sulfate-Based Diblock Copolymer Nanoparticles within Calcite: Effect of Varying the Surface Density of Anionic Stabilizer Chains

Yin Ning,[†] Lee A. Fielding,^{†,‡} Liam P. D. Ratcliffe,[†] Yun-Wei Wang,[§] Fiona C. Meldrum,[§] and Steven P. Armes^{*,†}

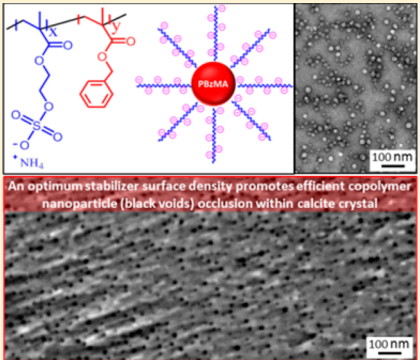
[†]Department of Chemistry, University of Sheffield, Brook Hill, Sheffield, South Yorkshire S3 7HF, U.K.

[‡]The School of Materials, University of Manchester, Oxford Road, Manchester, M13 9PL, U.K.

[§]School of Chemistry, University of Leeds, Leeds LS2 9JT, U.K.

Supporting Information

ABSTRACT: Polymerization-induced self-assembly (PISA) offers a highly versatile and efficient route to a wide range of organic nanoparticles. In this article, we demonstrate for the first time that poly(ammonium 2-sulfatoethyl methacrylate)-poly(benzyl methacrylate) [PSEM–PBzMA] diblock copolymer nanoparticles can be prepared with either a high or low PSEM stabilizer surface density using either RAFT dispersion polymerization in a 2:1 v/v ethanol/water mixture or RAFT aqueous emulsion polymerization, respectively. We then use these model nanoparticles to gain new insight into a key topic in materials chemistry: the occlusion of organic additives into inorganic crystals. Substantial differences are observed for the extent of occlusion of these two types of anionic nanoparticles into calcite (CaCO_3), which serves as a suitable model host crystal. A low PSEM stabilizer surface density leads to uniform nanoparticle occlusion within calcite at up to 7.5% w/w (16% v/v), while minimal occlusion occurs when using nanoparticles with a high PSEM stabilizer surface density. This counter-intuitive observation suggests that an optimum anionic surface density is required for efficient occlusion, which provides a hitherto unexpected design rule for the incorporation of nanoparticles within crystals.



INTRODUCTION

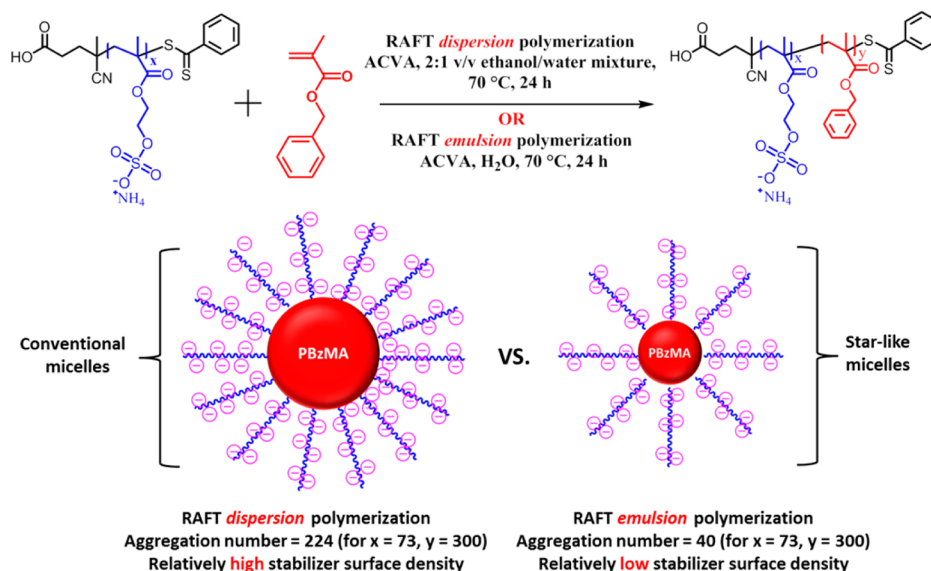
Biomaterials such as bones, teeth and seashells provide a wonderful demonstration of the remarkable control that organic molecules can achieve over inorganic crystal growth.^{1–4} Moreover, biomineralization is of considerable academic interest since it provides inspiration for the design of new synthetic organic/inorganic nanocomposite materials with superior toughness and hardness.^{5–12} In this context, exploring the molecular interaction between additives and inorganic hosts to gain a better understanding of the precise biomineralization mechanism is extremely important.^{13,14} However, this remains a formidable technical challenge. Inspired by Nature, various artificial biomaterials have been prepared by incorporating *soluble (macro)molecules* into inorganic crystals.^{15–20} However, the efficient occlusion of *nanoparticles* into inorganic crystals is much more difficult to achieve. For example, Wooley and co-workers used poly(acrylic acid)-stabilized copolymer nanoparticles as additives for the in situ crystallization of halite but found that these nanoparticles were solely located on the crystal surface.²¹ Recently, it has been demonstrated that nanoparticles decorated with suitable anionic carboxylate, phosphonate or sulfonate surface groups can be occluded within single crystals of calcite.^{6,9,10,22–26} Unfortunately, such nanoparticles required either intensive purification and/or derivatization prior to occlusion experi-

ments. Nevertheless, these studies are important, partly because incorporating significant quantities of nanoparticles into single crystals is counter-intuitive, but also because this represents a new route for the preparation of next-generation nanocomposite materials.^{6,9,10,22–31} However, a robust set of design rules for efficient occlusion remains elusive. Indeed, progress in this field to date has mainly relied on empirical trial-and-error experiments.

Clearly, the surface character of the nanoparticles must play a crucial role in occlusion because this dictates the nature of the host–guest interaction. However, the influence of surface chemistry on the extent of occlusion is poorly understood. This is in part because precise control over the nanoparticle surface chemistry is somewhat problematic when using conventional synthetic routes.^{9,10,22,23} Fortunately, polymerization-induced self-assembly (PISA) mediated by reversible addition–fragmentation chain transfer (RAFT) polymerization is a highly versatile technique that enables facile synthesis of a wide range of sterically stabilized diblock copolymer nanoparticles with controllable size, tunable morphology and adjustable surface functionality.^{32–37} Using this approach, a range of non-ionic,^{33,38–40} anionic,^{41,42} cationic^{43,44} or

Received: May 31, 2016

Published: August 10, 2016

Scheme 1^a

^aSynthesis of poly(ammonium 2-sulfatoethyl methacrylate)-poly(benzyl methacrylate) [PSEM-PBzMA] diblock copolymer nanoparticles at 10 % w/w solids by chain extension of a PSEM macro-CTA via either RAFT dispersion polymerization or RAFT aqueous emulsion polymerization of benzyl methacrylate (BzMA) at 70 °C for 24 h. The schematic cartoons indicate subtle differences in the mean aggregation number and stabilizer surface density when using these two PISA formulations, as discussed in the main text.

zwitterionic^{45–47} nanoparticles can be readily prepared in polar solvents (e.g., water or ethanol or mixtures thereof).

In this article we seek to precisely tune the surface composition of anionic diblock copolymer nanoparticles to extend our understanding of the design rules that govern nanoparticle occlusion within a model host crystal (calcite). More specifically, we show for the first time that PISA can be used to prepare copolymer nanoparticles with differing stabilizer surface densities. This is achieved by preparing poly(ammonium 2-sulfatoethyl methacrylate)-poly(benzyl methacrylate) [PSEM-PBzMA] nanoparticles using either RAFT dispersion polymerization in a 2:1 v/v ethanol/water mixture or RAFT aqueous emulsion polymerization (see Scheme 1). This approach offers an unprecedented opportunity to examine the relationship between the stabilizer surface density and the extent of nanoparticle occlusion. For the sake of brevity, a shorthand notation is utilized: PSEM and PBzMA denote the two blocks in the main text, while “S” and “B” respectively are used in figures, tables and captions. Thus, “S_x-B_y (emulsion)” denotes a PSEM_x-PBzMA_y diblock copolymer prepared by RAFT emulsion polymerization, where x and y indicate the mean degrees of polymerization (DP) of each block.

RESULTS AND DISCUSSION

Copolymer Synthesis and Characterization. Two PSEM macromolecular chain transfer agents (macro-CTAs) with mean DPs of either 32 or 73 were prepared via RAFT aqueous solution polymerization of ammonium 2-sulfatoethyl methacrylate (SEM) monomer. Gel permeation chromatography (GPC) studies confirmed that each macro-CTA had a relatively narrow molecular weight distribution ($M_w/M_n < 1.15$, see Figure S1, Supporting Information), which in principle enables the preparation of sterically stabilized nanoparticles with uniform corona thicknesses. Unfortunately, GPC cannot be used to analyze PSEM_x-PBzMA_y diblock copolymers

because no suitable eluent was available. Instead, chain extension experiments conducted using these PSEM macro-CTAs indicated high blocking efficiencies on addition of a further charge of SEM monomer, which suggests a high degree of RAFT end-group functionalization (see Figure S1a and S1b). These observations are consistent with UV–visible spectroscopy analysis, which indicated degrees of RAFT end-group functionalization of more than 99%, (see Figure S1c and S1d). As illustrated in Scheme 1, a series of anionic PSEM–PBzMA diblock copolymer nanoparticles were prepared by either RAFT dispersion polymerization in a 2:1 v/v ethanol/water mixture or RAFT aqueous emulsion polymerization. The BzMA conversion was monitored by ¹H NMR spectroscopy, which indicated that high conversions (>99%) were achieved after 24 h at 70 °C in all cases. Such PISA formulations enable the particle size to be readily controlled by systematic variation of the target DP of the core-forming block.^{24,29,48–50} Furthermore, the nature of the steric stabilizer block dictates the surface chemistry.^{41,43,50} Thus, in the present study choosing a PSEM macro-CTA should lead to anionic nanoparticles.

Figure 1 shows representative TEM images of sterically stabilized PSEM–PBzMA diblock copolymer nanoparticles prepared via PISA using either PSEM₃₂ or PSEM₇₃ macro-CTAs. In each case, the target DP of the core-forming PBzMA block was fixed at 300. However, the precise nature of the PISA formulation determines the final nanoparticle diameter.^{42,48,50,51} PSEM–PBzMA nanoparticles prepared via RAFT dispersion polymerization are significantly larger than those obtained by RAFT aqueous emulsion polymerization. This suggests a higher mean aggregation number in the former case (see Table 1), which is presumably because the repulsive electrostatic forces operating between neighboring copolymer chains are significantly weaker in a 2:1 ethanol/water mixture ($\epsilon_r \sim 43$ at 298 K) compared to pure water ($\epsilon_r = 79.5$ at the same temperature).⁵² Moreover, using a shorter PSEM stabilizer block for RAFT dispersion polymerization produces larger PSEM–PBzMA nanoparticles (compare Figure 1a and

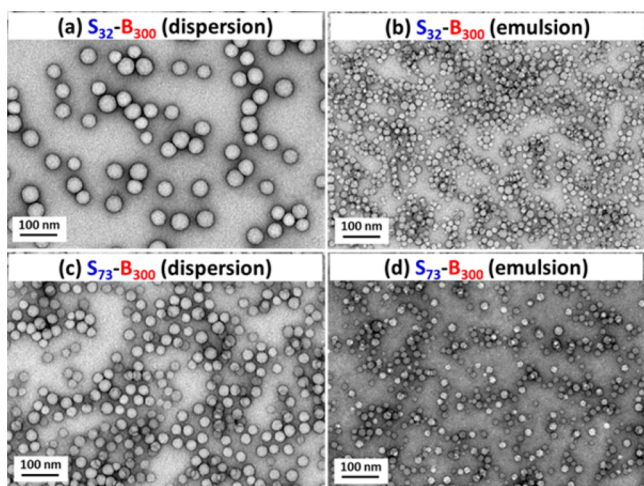


Figure 1. Representative TEM images obtained for various anionic diblock copolymer nanoparticles produced via RAFT-mediated PISA. (a) S_{32} - B_{300} (dispersion); (b) S_{32} - B_{300} (emulsion); (c) S_{73} - B_{300} (dispersion); (d) S_{73} - B_{300} (emulsion).

1c). Similar results have been reported for other PISA formulations.^{36,53}

Figure 2 shows dynamic light scattering (DLS) and aqueous electrophoresis data for various diblock copolymer nanoparticles as a function of either pH or Ca^{2+} concentration. According to Figure 2a, the hydrodynamic diameter of the nanoparticles is independent of the solution pH, which is indicative of good colloidal stability. Such behavior differs qualitatively from that of poly(methacrylic acid)-stabilized diblock copolymer nanoparticles, since in the latter case the weak polyelectrolyte stabilizer chains become protonated at low pH, resulting in aggregation.^{6,29} Figure 2b shows that PSEM_x-PBzMA_y diblock copolymer nanoparticles exhibit highly anionic pH-independent zeta potentials, as expected for a strong polyelectrolyte stabilizer.^{29,41,43} This pH-independent character

enables aggregation to be avoided during attempted occlusion, even if crystallization involves some variation in solution pH.²⁹ Comparing PSEM_x-PBzMA_y nanoparticles prepared by RAFT dispersion polymerization and RAFT emulsion polymerization, the former exhibit more negative zeta potentials than the latter. The physical reason for this difference in electrophoretic behavior is examined later. Although the zeta potential for the PSEM_x-PBzMA_y diblock copolymer nanoparticles is pH-independent, this parameter is affected by the addition of Ca^{2+} ions, even at a relatively low concentration (0.1 mM) as shown in Figure 2c. Indeed, all nanoparticles exhibit a significant reduction in zeta potential in the presence of Ca^{2+} , although an overall zeta potential of around -15 mV is maintained at 1.5 mM Ca^{2+} or higher. In addition, the intensity-average diameters recorded for S_{73} - B_{300} (emulsion) and S_{73} - B_{300} (dispersion) nanoparticles in the presence of 1.5 mM Ca^{2+} ions are slightly smaller than those determined in the absence of Ca^{2+} ions (see Figure S2). This is most likely due to charge screening caused by the presence of salt, although it is worth noting that the divalent Ca^{2+} cations do also bind strongly to the anionic sulfate groups on the PSEM stabilizer chains. Importantly, the presence of 1.5 mM Ca^{2+} ions does not cause any aggregation or precipitation (see Figure S2). Such PSEM stabilizer- Ca^{2+} ion interactions are likely to be important for occlusion during in situ crystallization, because they should promote nanoparticle adsorption onto the crystal surface.^{6,9,24}

Calcium Carbonate Precipitation. Calcium carbonate crystals were precipitated at pH 8–9 by exposing an aqueous solution containing $[Ca^{2+}] = 1.5$ mM and 0.0–0.10% w/w anionic diblock copolymer nanoparticles to ammonium carbonate vapor at 20 °C for 24 h.⁵⁴ A mixture of calcite and vaterite was precipitated at a copolymer concentration of 0.10% w/w (Figure S3), which is consistent with previous reports.^{6,9,22} Thus, a lower copolymer concentration of 0.01% w/w was selected for more detailed studies. Precipitation under the above conditions yielded 30–50 μ m rhombohedral calcite crystals in either the absence or presence of PSEM-PBzMA

Table 1. Summary of TEM Diameters, DLS Diameters, XPS Elemental Compositions, Mean Aggregation Numbers and Calculated PSEM Stabilizer Surface Densities Obtained for Various Diblock Copolymer Nanoparticles Prepared via PISA

sample ID	TEM diameter (nm) ^a	DLS diameter (nm)	XPS data				aggregation number (N_{agg}) ^c	stabilizer surface density (10^{-2} chain per nm^2) ^d
			S2p atom %	C1s atom %	S2p/C1s atomic ratio (10^{-3})	normalized S2p/C1s atomic ratio (%) ^b		
S_{32} homopolymer	N/A	N/A	8.2	47.6	172.3 ^f	100.0	N/A	N/A
S_{32} - B_{300} (dispersion)	56 ± 5	80 (0.07) ^e	1.3	74.2	17.5	10.6	1204	10.9
S_{32} - B_{300} (emulsion)	18 ± 4	31 (0.12)	0.7	71.8	9.7	5.9	40	3.4
S_{32} - B_{500} (dispersion)	100 ± 16	129 (0.03)	1.6	73.4	21.8	13.2	4114	12.4
S_{32} - B_{500} (emulsion)	26 ± 6	36 (0.17)	0.6	72.4	8.3	5.0	72	3.2
S_{73} homopolymer	N/A	N/A	8.3	48.5	171.1 ^f	100.0	N/A	N/A
S_{73} - B_{100} (dispersion)	19 ± 2	42 (0.27)	1.5	73.2	20.5	12.0	141	6.5
S_{73} - B_{300} (dispersion)	32 ± 3	52 (0.07)	1.3	72.1	18.0	10.5	224	5.4
S_{73} - B_{300} (emulsion)	18 ± 3	35 (0.10)	0.7	78.8	8.9	5.2	40	3.1
S_{73} - B_{500} (dispersion)	53 ± 12	96 (0.07)	1.4	74.9	18.7	10.9	612	6.0
S_{73} - B_{500} (emulsion)	21 ± 4	45 (0.27)	0.6	73.4	8.2	4.8	38	2.3
[0.5 S_{73} + 0.5 G_{70}]- B_{300} (emulsion)	21 ± 3	45 (0.22)	0.4	72.4	5.5	3.2	64	1.9 ^g
PBzMA ₃₀₀	N/A	N/A	0.0	84.9	0.0	0	N/A	N/A

^aMean TEM diameter determined by analyzing more than 200 particles using ImageJ software. ^b $[S2p/C1s \text{ (particle)}]/[S2p/C1s \text{ (stabilizer)}]$ (%). ^cFurther details of the calculation of this parameter can be found in the Supporting Information (see page S10). ^dStabilizer surface density was calculated using eq 1, which is derived in the Supporting Information. ^eThe number in brackets represents the DLS polydispersity. ^fTheoretical values are 175.3 and 170.5 for S_{32} and S_{73} , respectively. ^gThere are two types of stabilizer in this case; the calculated value refers only to the PSEM₇₃ chains to aid comparison.

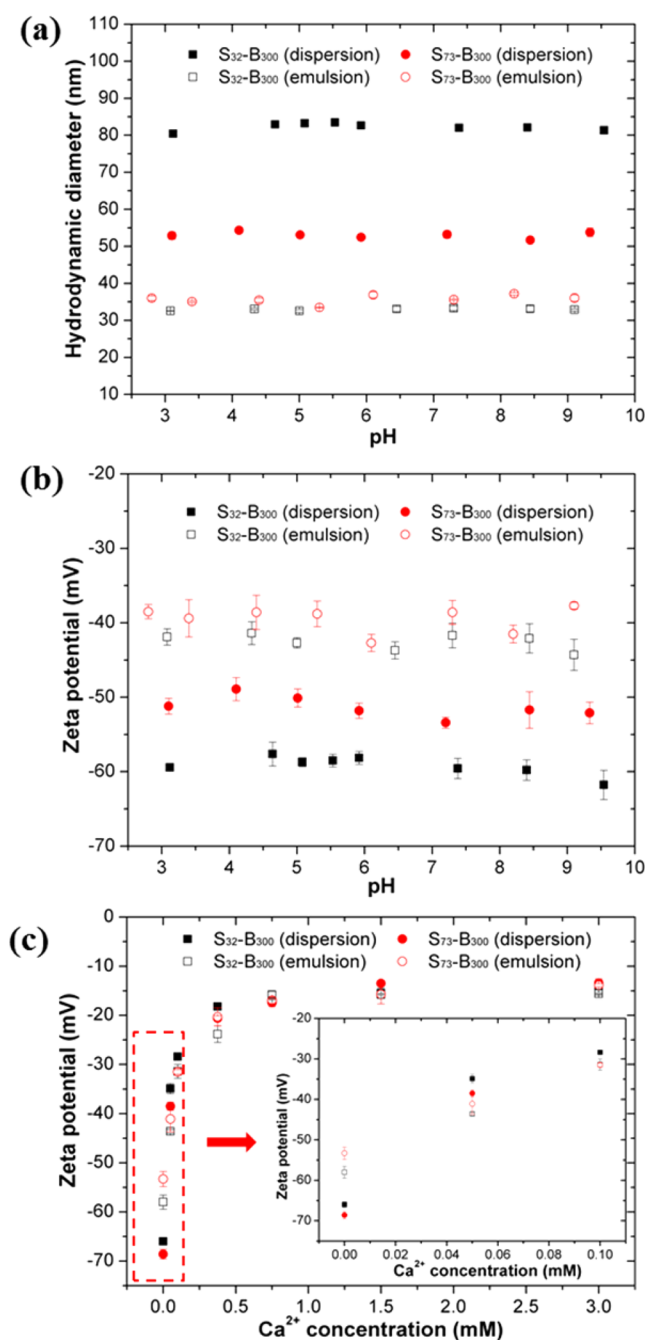


Figure 2. Dynamic light scattering and aqueous electrophoresis data obtained for spherical diblock copolymer nanoparticles conducted at a copolymer concentration of $\sim 0.1\%$ w/w: (a) hydrodynamic diameter vs pH; (b) zeta potential vs pH in the presence of 1 mM NaCl as background electrolyte; and (c) zeta potential vs Ca^{2+} concentration, conducted at a copolymer nanoparticle concentration of 0.01% w/w (which corresponds to the occlusion conditions). The inset in (c) shows the zeta potentials observed for nanoparticles at Ca^{2+} concentrations ranging from 0 to 0.15 mM.

diblock copolymer nanoparticles or PSEM₇₃ homopolymer, see Figure S4. Characteristic Raman bands were detected at 154 and 280 cm^{-1} (lattice modes), 712 cm^{-1} (ν_4) and 1086 cm^{-1} (ν_1) for both calcite control and copolymer/calcite nanocomposite (Figure S5).^{54,55}

Particle occlusion within calcite was investigated by imaging fractured crystals with field emission electron scanning

microscopy (FE-SEM, Figure 3). It is worth noting that no occlusion was observed for poly(glycerol monomethacrylate)₇₀-poly(benzyl methacrylate)₃₀₀ (PGMA₇₀-PBzMA₃₀₀) copolymer nanoparticles, as expected (see Scheme S1a and Figure S6). This is because the poly(glycerol monomethacrylate) (G₇₀) stabilizer is non-ionic, hence there is no favorable electrostatic interaction with the growing crystal. However, some degree of occlusion did occur when 50% of the non-ionic PGMA₇₀ stabilizer chains were replaced with anionic PSEM₇₃ stabilizer for the synthesis of [0.5 PSEM₇₃ + 0.5 PGMA₇₀]-B₃₀₀ (emulsion) nanoparticles, see Scheme S1b and Figure S7. Random occlusion was observed for PSEM₃₂-PBzMA₃₀₀ and PSEM₇₃-PBzMA₃₀₀ nanoparticles prepared via RAFT dispersion polymerization, but such incorporation appears to be rather inhomogeneous (see Figure 3a and 3b, and corresponding low magnification images in Figure S8). In contrast, the PSEM₃₂-PBzMA₃₀₀ and PSEM₇₃-PBzMA₃₀₀ nanoparticles obtained using RAFT aqueous emulsion polymerization are much more uniformly incorporated within calcite (see Figure 3c–g).

The calcite crystals precipitated in the presence of 0.01% w/w PSEM₇₃-PBzMA₃₀₀ (emulsion) were examined in more detail. The internal structure of a fractured crystal is shown in Figure 3d–g: these images demonstrate that the nanoparticles are both non-aggregated and uniformly occluded throughout the crystal. It is also noteworthy that all nanoparticle cavities are spherical and comparable in size to the original PSEM₇₃-PBzMA₃₀₀ (emulsion) nanoparticles (Figure 3g). Kim et al. previously reported that relatively soft anionic diblock copolymer spherical micelles deform and flatten during their occlusion into calcite.⁹ This phenomenon was recently studied in detail by Cho et al., who used atomic force microscopy (AFM) and micromechanical simulations to rationalize the in situ change in copolymer morphology.²⁵ Presumably, the relatively high glass transition temperature of the PBzMA core-forming block prevents deformation of the PSEM₇₃-PBzMA₃₀₀ (emulsion) nanoparticles examined in the present work.

The extent of occlusion was quantified using thermogravimetric analysis (TGA, Figure 4) which showed that the PSEM₇₃-PBzMA₃₀₀ (emulsion) diblock copolymer nanoparticles were completely pyrolyzed on heating in air up to 550 °C. Pure calcite decomposed to give a CaO residue of 56.4% by mass, which is close to its theoretical CaO content of 56.0%. Based on these data, it is calculated that the occlusion is almost negligible for PSEM₇₃-PBzMA₃₀₀ (dispersion) nanoparticles. For the [0.5 PSEM₇₃ + 0.5 PGMA₇₀]-PBzMA₃₀₀ nanoparticles, the extent of occlusion is $\sim 2\%$ w/w. The TGA curve obtained for the PSEM₇₃-PBzMA₃₀₀ (emulsion)/calcite nanocomposite crystals exhibited three distinct features. First, a 3.7% mass loss was observed up to 600 °C which is assigned to decomposition of PSEM₇₃-PBzMA₃₀₀ (emulsion) nanoparticles located in the outer regions of the host crystal. Second, the TGA curve was shifted to a higher temperature, suggesting enhanced thermal stability for the nanocomposite crystal. Finally, the 52.2% residue obtained at 850 °C is significantly lower than that observed for pure calcite (56.4%), which indicates successful occlusion. The degree of occlusion calculated for PSEM₇₃-PBzMA₃₀₀ nanoparticles is 7.5% w/w, or approximately 16% v/v (assuming a copolymer density of 1.18 g cm^{-3} , as determined by helium pycnometry; see Supporting Information for the detailed calculation). The occlusion of PSEM₇₃-PBzMA₃₀₀ (emulsion) diblock copolymer nanoparticles within calcite was also confirmed by FT-IR

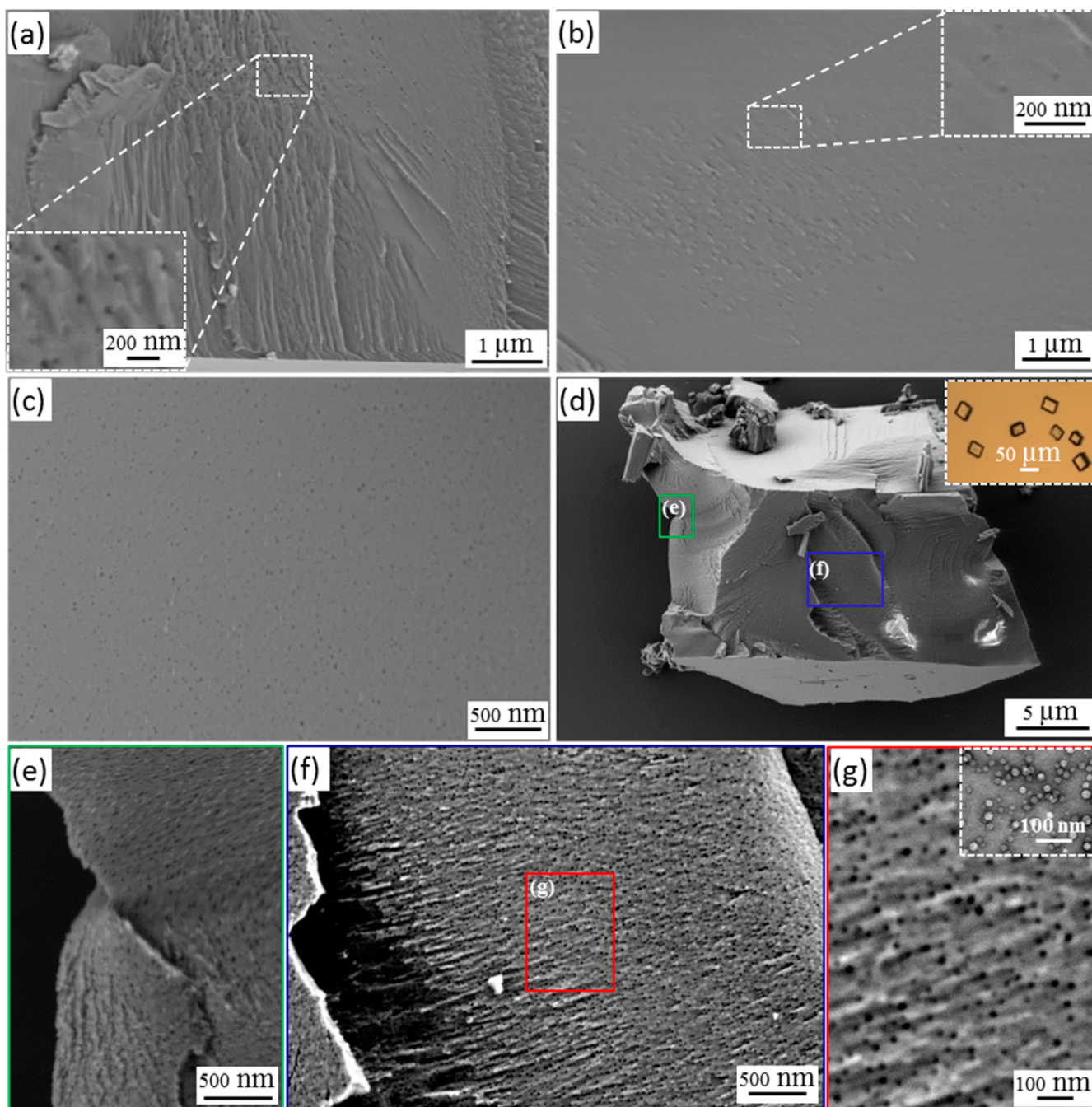


Figure 3. Representative FE-SEM images obtained for fractured calcium carbonate crystals prepared in the presence of (a) S_{32} - B_{300} (dispersion) and (b) S_{73} - B_{300} (dispersion) nanoparticles at a fixed copolymer concentration of 0.01% w/w. The insets in (a) and (b) are magnified images corresponding to the labeled rectangular areas. In both cases only relatively low levels of occlusion are observed (further corresponding low magnification FE-SEM images are provided in Figure S8). FE-SEM images for (c) S_{32} - B_{300} (emulsion) and (d) S_{73} - B_{300} (emulsion) show fractured crystals at low magnification. The inset in (d) shows an optical micrograph obtained for intact rhombohedral calcite crystals prior to fracture. (e) and (f) depict magnified images of selected areas as indicated in (d), confirming that such nanoparticles are efficiently and uniformly occluded within calcium carbonate crystals. (g) Magnified image showing the rectangular area indicated in (f). The inset in (g) is a TEM image obtained for the S_{73} - B_{300} (emulsion) nanoparticles prior to their occlusion. Clearly, the dimensions of the occluded features observed in (g) are consistent with the diameter of the original nanoparticles.

spectroscopy, since the ester carbonyl band assigned to PSEM₇₃-PBzMA₃₀₀ was detected as a weak feature in the FT-IR spectrum recorded for the PSEM₇₃-PBzMA₃₀₀ (emulsion)/calcite nanocomposite crystals (see Figure S9).

Investigation of Nanoparticle Occlusion Behavior. On the basis of studies to date, anionic nanoparticles comprising carboxylate, phosphonate or sulfonate surface functional groups

can be occluded within inorganic crystals such as calcite^{6,9,10,22–26} or ZnO.^{29,30} However, the essential criteria required for efficient occlusion are not yet understood. Hence progress in this field has been hitherto mainly based on empirical trial-and-error experiments. Thus, elucidation of a robust set of design rules is highly desirable, both for

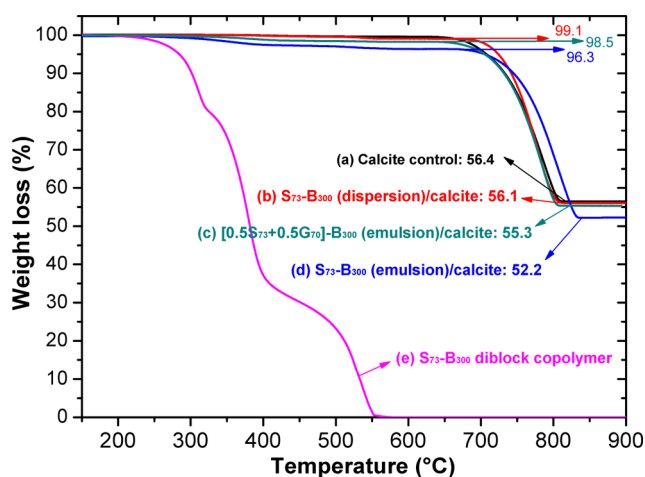


Figure 4. Thermogravimetric analysis (TGA) data obtained for S_{73} – B_{300} /calcite nanocomposite crystals and corresponding control samples. (a) Calcite control, showing the expected approximate 44% mass loss as a result of CaO formation via loss of CO_2 . (b) S_{73} – B_{300} (dispersion)/calcite nanocomposite crystals exhibit a slightly greater weight loss compared to the calcite control; this indicates a relatively low level of copolymer nanoparticle occlusion and is consistent with FE-SEM studies (see Figure 3b). (c) $[0.5 S_{73} + 0.5 G_{73}]$ – B_{300} (emulsion)/calcite nanocomposite crystals. (d) S_{73} – B_{300} (emulsion)/calcite nanocomposite crystals exhibit a significantly greater weight loss. (e) Original S_{73} – B_{300} diblock copolymer nanoparticles, indicating complete pyrolysis of this purely organic component.

optimizing the occlusion efficiency and also for extending occlusion to include alternative inorganic host crystals.

These two sets of nanoparticles possess apparently the same surface chemistry but exhibit substantial differences with regard to their extents of occlusion within calcite. Initially, this discrepancy was considered to be possibly a particle size effect. However, control experiments ruled out this hypothesis. More specifically, a series of PSEM_x – PBzMA_y (dispersion) nanoparticles ranging in size from 18 to 100 nm diameter were prepared by varying the PBzMA DP at 10% w/w solids and evaluated for occlusion into calcite under the same conditions. Remarkably, all PSEM_x – PBzMA_y nanoparticles prepared by RAFT dispersion polymerization are either not occluded or only weakly occluded within calcite (see Figure S10), whereas all PSEM_x – PBzMA_y nanoparticles prepared by RAFT emulsion polymerization can be uniformly incorporated into calcite regardless of their particle size (see Figure 3c–g and Figure S11). Thus, it seems that occlusion is not sensitive to the nanoparticle dimensions, at least over the 18 to 100 nm size range studied here. In fact, Kim and co-workers reported that anionic carboxylated latexes of approximately 220–250 nm diameter could be occluded within calcite.¹⁰ Moreover, occlusion does not appear to be particularly sensitive to the stabilizer DP because both PSEM_{32} – PBzMA_y and PSEM_{73} – PBzMA_y nanoparticles prepared via RAFT aqueous emulsion polymerization can be uniformly occluded within calcite, see Figure 3c,d, and Figure S11.

As discussed above, the zeta potential for nanoparticles prepared by RAFT dispersion polymerization is significantly more negative than that for nanoparticles prepared via RAFT aqueous emulsion polymerization (see Figure 2b). This observation led us to determine the stabilizer surface densities for these two types of nanoparticles, because we hypothesized

that this parameter might explain their differing occlusion behavior.

Assuming perfect blocking efficiency, full BzMA conversion and a relatively narrow particle size distribution, the stabilizer surface density can be calculated using eq 1 (see Supporting Information for a derivation):

$$D_s = \frac{n_{\text{PSEM}} N_A \rho r}{3(m_s + m_b)} \times 10^{-21} \quad (1)$$

Here D_s is the stabilizer surface density expressed as the number of chains per nm^2 and n_{PSEM} , N_A , ρ and r denote the number of moles of PSEM macro-CTA (mol), Avogadro's number (mol^{-1}), the solid-state density of the dried nanoparticles (g cm^{-3}) and the mean nanoparticle radius (nm), respectively. The masses (g) of the PSEM macro-CTA and PBzMA are given by m_s and m_b , respectively.

Using eq 1, the stabilizer surface densities of the diblock copolymer nanoparticles were determined from the nanoparticle dimensions and these data are summarized in Table 1. In all cases, PSEM_x – PBzMA_y nanoparticles prepared via RAFT dispersion polymerization have significantly higher surface stabilizer densities than the corresponding nanoparticles prepared via RAFT emulsion polymerization. Direct experimental evidence of this finding was also provided by X-ray photoelectron spectroscopy (XPS), which is an established analytical technique for determining surface chemical compositions. XPS has excellent inter-element resolution and is highly surface-specific, with a typical sampling depth of 2–10 nm.⁵⁶ For the current study, the PSEM stabilizer chains provide a unique source of sulfur atoms. Hence higher sulfur contents indicate higher stabilizer surface densities (see Figure 5). Both

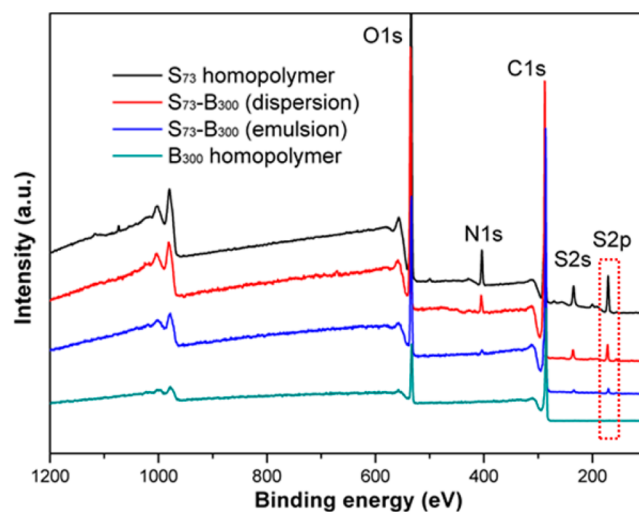


Figure 5. X-ray photoelectron survey spectra recorded for a S_{73} homopolymer control, S_{73} – B_{300} (dispersion), S_{73} – B_{300} (emulsion), and a B_{300} homopolymer control. The red rectangle highlights the relative $\text{S}2p$ intensities, which are in the order: B_{300} homopolymer < S_{73} – B_{300} (emulsion) < S_{73} – B_{300} (dispersion) < S_{73} homopolymer.

the PSEM stabilizer and the PBzMA core-forming block contain carbon atoms, which give rise to $\text{C}1s$ signals in XPS. All samples were run under the same conditions and the $\text{S}2p/\text{C}1s$ atomic ratios calculated from XPS analysis of the S_x homopolymers are very close to theoretical values (see Table 1). Thus, the level of surface carbon contamination is low (and assumed to be negligible). Normalized atomic ratios [i.e., $\text{S}2p/$

C1s (particle)]/[S2p/C1s (stabilizer)] were calculated to compare stabilizer surface densities for the nanoparticles, as summarized in Table 1. As expected, no sulfur signals were detected for the PBzMA₃₀₀ control and the PSEM₇₃ control had the highest sulfur content (strongest S2p signal). More importantly, PSEM_x-PBzMA_y nanoparticles prepared via RAFT dispersion polymerization exhibited consistently higher normalized [S2p/C1s (particle)]/[S2p/C1s (stabilizer)] atomic ratios (by a factor of approximately two) compared to the equivalent nanoparticles prepared via RAFT emulsion polymerization. This indicates that the former nanoparticles have a higher stabilizer surface density than the latter. This difference is consistent with the theoretical stabilizer surface densities calculated using eq 1 and can be ascribed to two reasons. First, the relatively low dielectric constant for the 2:1 v/v ethanol/water mixture (compared to pure water) reduces electrostatic repulsion between neighboring highly anionic PSEM stabilizers during nanoparticle formation via PISA, which results in a more densely packed coronal layer. Second, the PBzMA chains are likely to be slightly more solvated (and hence more stretched, leading to more closely packed copolymer chains in the nanoparticle cores) when grown in the 2:1 v/v ethanol/water mixture, compared to PISA syntheses conducted in pure water.⁵⁷ One reviewer of this manuscript suggested that the higher stabilizer surface density observed for PSEM₇₃-PBzMA₃₀₀ (dispersion) might be the result of a significant change in core solvation during dialysis against water. However, both literature data⁵⁷ and DLS studies conducted before and after dialysis do not support this hypothesis, because only a rather small change in the intensity-average particle diameter is observed (see Figure S12).

Naively, a higher stabilizer surface density should provide stronger nanoparticle binding to the crystal surface and hence lead to higher levels of occlusion. However, *less* occlusion is actually observed, which at first sight appears to be counter-intuitive. The present study shows that *efficient* occlusion actually requires an *optimum* (rather than maximum) stabilizer surface density. A tentative occlusion mechanism is as follows. Prior to precipitation of calcium carbonate, Ca²⁺ ions bind to the anionic stabilizer chains of PSEM_x-PBzMA_y nanoparticles in aqueous solution, as indicated by their significantly less anionic zeta potential compared to nanoparticles in the absence of Ca²⁺ (see Figure 2c). Under otherwise identical conditions (i.e., 1.5 mM Ca²⁺ and 0.01% w/w copolymer at 20 °C), the extent of Ca²⁺ ion binding to the anionic sulfate groups on the PSEM₇₃-PBzMA₃₀₀ (emulsion) and PSEM₇₃-PBzMA₃₀₀ (dispersion) nanoparticles is estimated to be 5.9 ± 1.2 mg g⁻¹ and 6.1 ± 1.4 mg g⁻¹ respectively, as determined using a calcium ion-selective electrode (see Figure S13).⁵⁸ If the stabilizer chains are closely packed, the relatively high stabilizer surface density means that Ca²⁺ ions primarily act as ionic cross-linkers between adjacent PSEM chains. Thus, the ensuing loss of conformational entropy reduces the ability of these sterically stabilized nanoparticles to interact with the growing crystal, see Figure 6a. However, such ionic cross-linking is much less likely to occur if the stabilizer surface density is relatively low, which allows the nanoparticles prepared via RAFT emulsion polymerization to retain more conformational entropy. Hence a greater proportion of the stabilizer chains are able to relax, which enables these nanoparticles to bind more strongly on the growing calcite surface (see Figure 6b). This interpretation is consistent with recent in situ AFM studies, which demonstrate that anionic block copolymer micelles uniquely bind at calcite

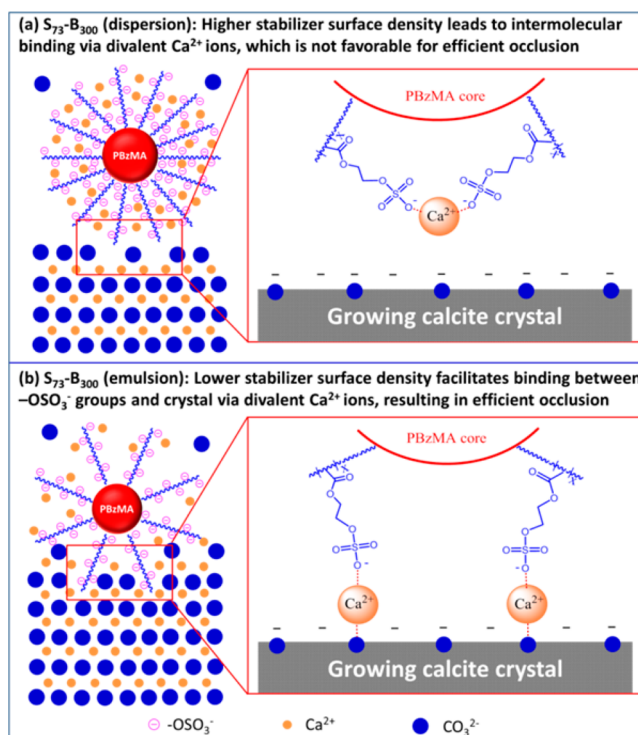


Figure 6. Schematic cartoon representing the proposed occlusion mechanism. (a) Crystallization in the presence of S_x-B_y (dispersion) nanoparticles. The relatively high stabilizer surface density means that Ca^{2+} ions primarily act as ionic cross-linkers between adjacent stabilizer chains and the ensuing loss of conformational entropy reduces nanoparticle interactions with the growing crystal. (b) Crystallization in the presence of S_x-B_y (emulsion) nanoparticles. In this case the relatively low stabilizer density reduces the degree of ionic cross-linking between stabilizer chains and enables the nanoparticles to interact more strongly with the growing crystals, hence promoting efficient occlusion.

step edges prior to their incorporation.²⁵ A further reduction in the PSEM stabilizer surface density can be achieved by introducing non-ionic PGMA stabilizer chains. Such [0.5 PSEM₇₃ + 0.5 PGMA₇₀]-B₃₀₀ (emulsion) nanoparticles exhibit an extent of occlusion of just 2% w/w. One possible explanation is that the presence of the non-ionic PGMA stabilizer chains restricts the ability of the anionic PSEM stabilizer chains to interact efficiently with the growing calcite crystals. Alternatively, the (diluted) PSEM surface density may be simply too low to ensure efficient interaction between such copolymer nanoparticles and the growing calcite crystals.

To examine the effect of varying stabilizer surface density for other inorganic crystal hosts, we also performed some preliminary occlusion experiments using ZnO instead of calcite. PSEM₇₃-PBzMA₃₀₀ nanoparticles prepared by RAFT emulsion polymerization exhibited a significantly higher extent of occlusion (13.9% w/w vs 7.2% w/w, see Figure S14) compared to PSEM₇₃-PBzMA₁₀₀ (dispersion) nanoparticles of comparable size. This is in good agreement with the calcite system and further suggests that an *optimum* stabilizer surface density is required to *maximize* the extent of occlusion.

CONCLUSIONS

In summary, a range of well-defined highly anionic diblock copolymer nanoparticles with tunable surface chemistry have been prepared via RAFT-mediated PISA. The stabilizer surface

density depends on the solvent quality for the stabilizer chains, which offers an unprecedented opportunity to examine the relationship between nanoparticle surface functionality and the corresponding extent of occlusion within calcite crystals. Up to 7.5% w/w (or ~16% v/v) PSEM₇₃-PBzMA₃₀₀ (emulsion) nanoparticles can be incorporated within calcite (CaCO₃) even when using a relatively low copolymer concentration (0.01% w/w). Surprisingly, more anionic nanoparticles prepared via RAFT dispersion polymerization using a 2:1 v/v ethanol/water mixture are occluded much less efficiently into calcite under identical crystallization conditions. This suggests that there is an *optimum* (rather than a maximum) surface density of anionic stabilizer chains for occlusion into this host crystal. Thus, this work provides important new insights regarding the rather subtle role played by the nanoparticle surface chemistry in determining occlusion efficiencies within calcite. Moreover, our findings are expected to inform the design of new organic/inorganic nanocomposite crystals.

■ ASSOCIATED CONTENT

● Supporting Information

The Supporting Information is available free of charge on the ACS Publications website at DOI: 10.1021/jacs.6b05563.

Experimental details and characterization methods, scheme, GPC data, UV-visible spectra, optical micrographs, DLS data, FE-SEM images, Raman spectra and theoretical calculation of aggregation number and stabilizer surface density (PDF)

■ AUTHOR INFORMATION

Corresponding Author

*s.p.arnes@sheffield.ac.uk

Notes

The authors declare no competing financial interest.

■ ACKNOWLEDGMENTS

The Overseas Study Program of Guangzhou Elite Project is thanked for sponsorship of a PhD studentship for Y. Ning. Prof Graham Leggett and Dr. Deborah Hammond are thanked for their assistance and technical advice on the XPS studies. We thank EPSRC for postdoctoral support (EP/J018589/1 and EP/K006304/1). SPA also acknowledges a five-year ERC Advanced Investigator grant (PISA 320372).

■ REFERENCES

- (1) Belcher, A. M.; Wu, X. H.; Christensen, R. J.; Hansma, P. K.; Stucky, G. D.; Morse, D. E. *Nature* **1996**, *381*, 56–58.
- (2) Berman, A.; Hanson, J.; Leiserowitz, L.; Koetzle, T. F.; Weiner, S.; Addadi, L. *Science* **1993**, *259*, 776–779.
- (3) Mann, S. *Biomaterialization, Principles and Concepts in Bioinorganic Materials Chemistry*; Oxford University Press: Oxford, 2001.
- (4) Lowenstam, H. A.; Weiner, S. *On Biomaterialization*; Oxford University Press: New York, 1989.
- (5) Berman, A.; Addadi, L.; Kvick, A.; Leiserowitz, L.; Nelson, M.; Weiner, S. *Science* **1990**, *250*, 664–667.
- (6) Kim, Y.-Y.; Semsarilar, M.; Carloni, J. D.; Cho, K. R.; Kulak, A. N.; Polishchuk, I.; Hendley, C. T.; Smeets, P. J. M.; Fielding, L. A.; Pokroy, B.; Tang, C. C.; Estroff, L. A.; Baker, S. P.; Armes, S. P.; Meldrum, F. C. *Adv. Funct. Mater.* **2016**, *26*, 1382–1392.
- (7) Kim, Y.-Y.; Carloni, J. D.; Demarchi, B.; Sparks, D.; Reid, D. G.; Kunitake, M. E.; Tang, C. C.; Duer, M. J.; Freeman, C. L.; Pokroy, B.; Penkman, J. H. H.; Estroff, L. A.; Baker, S. P.; Meldrum, F. C. *Nat. Mater.* **2016**, *15*, 903–910.
- (8) Kim, Y. Y.; Schenk, A. S.; Walsh, D.; Kulak, A. N.; Cespedes, O.; Meldrum, F. C. *Nanoscale* **2014**, *6*, 852–859.
- (9) Kim, Y.-Y.; Ganesan, K.; Yang, P.; Kulak, A. N.; Borukhin, S.; Pechook, S.; Ribeiro, L.; Kroeger, R.; Eichhorn, S. J.; Armes, S. P.; Pokroy, B.; Meldrum, F. C. *Nat. Mater.* **2011**, *10*, 890–896.
- (10) Kim, Y.-Y.; Ribeiro, L.; Maillot, F.; Ward, O.; Eichhorn, S. J.; Meldrum, F. C. *Adv. Mater.* **2010**, *22*, 2082–2086.
- (11) Meldrum, F. C.; Cölfen, H. *Chem. Rev.* **2008**, *108*, 4332–4432.
- (12) Dunlop, J. W.; Fratzl, P. *Annu. Rev. Mater. Res.* **2010**, *40*, 1–24.
- (13) Li, H.; Xin, H. L.; Muller, D. A.; Estroff, L. A. *Science* **2009**, *326*, 1244–1247.
- (14) Orme, C. A.; Noy, A.; Wierzbicki, A.; McBride, M. T.; Grantham, M.; Teng, H. H.; Dove, P. M.; DeYoreo, J. J. *Nature* **2001**, *411*, 775–779.
- (15) Metzler, R. A.; Tribello, G. A.; Parrinello, M.; Gilbert, P. U. P. A. *J. Am. Chem. Soc.* **2010**, *132*, 11585–11591.
- (16) Yu, S. H.; Cölfen, H. *J. Mater. Chem.* **2004**, *14*, 2124–2147.
- (17) Teng, H. H.; Dove, P. M.; Orme, C. A.; De Yoreo, J. J. *Science* **1998**, *282*, 724–727.
- (18) Li, H.; Estroff, L. A. *Adv. Mater.* **2009**, *21*, 470–473.
- (19) Aizenberg, J.; Hanson, J.; Koetzle, T. F.; Weiner, S.; Addadi, L. *J. Am. Chem. Soc.* **1997**, *119*, 881–886.
- (20) Nudelman, F.; Sommerdijk, N. *Angew. Chem., Int. Ed.* **2012**, *51*, 6582–6596.
- (21) Pasteris, J. D.; Freeman, J. J.; Wopenka, B.; Qi, K.; Ma, Q.; Wooley, K. L. *Astrobiology* **2006**, *6*, 625–643.
- (22) Kulak, A. N.; Semsarilar, M.; Kim, Y.-Y.; Ihli, J.; Fielding, L. A.; Cespedes, O.; Armes, S. P.; Meldrum, F. C. *Chem. Sci.* **2014**, *5*, 738–743.
- (23) Kulak, A. N.; Yang, P.; Kim, Y.-Y.; Armes, S. P.; Meldrum, F. C. *Chem. Commun.* **2014**, *50*, 67–69.
- (24) Ning, Y.; Fielding, L. A.; Doncom, K. E. B.; Penfold, N. J. W.; Kulak, A. N.; Matsuoka, H.; Armes, S. P. *ACS Macro Lett.* **2016**, *5*, 311–315.
- (25) Rae Cho, K.; Kim, Y.-Y.; Yang, P.; Cai, W.; Pan, H.; Kulak, A. N.; Lau, J. L.; Kulshreshtha, P.; Armes, S. P.; Meldrum, F. C.; De Yoreo, J. J. *Nat. Commun.* **2016**, *7*, 10187.
- (26) Hanisich, A.; Yang, P.; Kulak, A. N.; Fielding, L. A.; Meldrum, F. C.; Armes, S. P. *Macromolecules* **2016**, *49*, 192–204.
- (27) Lu, C. H.; Qi, L. M.; Cong, H. L.; Wang, X. Y.; Yang, J. H.; Yang, L. L.; Zhang, D. Y.; Ma, J. M.; Cao, W. X. *Chem. Mater.* **2005**, *17*, 5218–5224.
- (28) Li, C.; Qi, L. *Angew. Chem., Int. Ed.* **2008**, *47*, 2388–2393.
- (29) Ning, Y.; Fielding, L. A.; Andrews, T. S.; Growney, D. J.; Armes, S. P. *Nanoscale* **2015**, *7*, 6691–6702.
- (30) Muñoz-Espí, R.; Qi, Y.; Lieberwirth, I.; Gómez, C. M.; Wegner, G. *Chem. - Eur. J.* **2006**, *12*, 118–129.
- (31) Liu, Y.; Yuan, W.; Shi, Y.; Chen, X.; Wang, Y.; Chen, H.; Li, H. *Angew. Chem., Int. Ed.* **2014**, *53*, 4127–4131.
- (32) Zhang, L. F.; Eisenberg, A. *Science* **1995**, *268*, 1728–1731.
- (33) Li, Y.; Armes, S. P. *Angew. Chem., Int. Ed.* **2010**, *49*, 4042–4046.
- (34) Blanazs, A.; Armes, S. P.; Ryan, A. J. *Macromol. Rapid Commun.* **2009**, *30*, 267–277.
- (35) Warren, N. J.; Armes, S. P. *J. Am. Chem. Soc.* **2014**, *136*, 10174–10185.
- (36) Fielding, L. A.; Derry, M. J.; Ladmiral, V.; Rosselgong, J.; Rodrigues, A. M.; Ratcliffe, L. P. D.; Sugihara, S.; Armes, S. P. *Chem. Sci.* **2013**, *4*, 2081–2087.
- (37) Derry, M. J.; Fielding, L. A.; Armes, S. P. *Prog. Polym. Sci.* **2016**, *52*, 1–18.
- (38) Blanazs, A.; Verber, R.; Mykhaylyk, O. O.; Ryan, A. J.; Heath, J. Z.; Douglas, C. W. I.; Armes, S. P. *J. Am. Chem. Soc.* **2012**, *134*, 9741–9748.
- (39) Blanazs, A.; Ryan, A. J.; Armes, S. P. *Macromolecules* **2012**, *45*, 5099–5107.
- (40) Blanazs, A.; Madsen, J.; Battaglia, G.; Ryan, A. J.; Armes, S. P. *J. Am. Chem. Soc.* **2011**, *133*, 16581–16587.
- (41) Semsarilar, M.; Ladmiral, V.; Blanazs, A.; Armes, S. P. *Langmuir* **2012**, *28*, 914–922.

- (42) Semsarilar, M.; Jones, E. R.; Blanazs, A.; Armes, S. P. *Adv. Mater.* **2012**, *24*, 3378–3382.
- (43) Semsarilar, M.; Ladmiral, V.; Blanazs, A.; Armes, S. P. *Langmuir* **2013**, *29*, 7416–7424.
- (44) Smith, A. E.; Xu, X.; Kirkland-York, S. E.; Savin, D. A.; McCormick, C. L. *Macromolecules* **2010**, *43*, 1210–1217.
- (45) Doncom, K. E. B.; Warren, N. J.; Armes, S. P. *Polym. Chem.* **2015**, *6*, 7264–7273.
- (46) Sugihara, S.; Blanazs, A.; Armes, S. P.; Ryan, A. J.; Lewis, A. L. *J. Am. Chem. Soc.* **2011**, *133*, 15707–15713.
- (47) Sun, J.-T.; Yu, Z.-Q.; Hong, C.-Y.; Pan, C.-Y. *Macromol. Rapid Commun.* **2012**, *33*, 811–818.
- (48) Zhang, X.; Rieger, J.; Charleux, B. *Polym. Chem.* **2012**, *3*, 1502–1509.
- (49) Chaduc, I.; Crepet, A.; Boyron, O.; Charleux, B.; D'Agosto, F.; Lansalot, M. *Macromolecules* **2013**, *46*, 6013–6023.
- (50) Cunningham, V. J.; Alswieleh, A. M.; Thompson, K. L.; Williams, M.; Leggett, G. J.; Armes, S. P.; Musa, O. M. *Macromolecules* **2014**, *47*, 5613–5623.
- (51) Boisse, S.; Rieger, J.; Pembouong, G.; Beaunier, P.; Charleux, B. *J. Polym. Sci., Part A: Polym. Chem.* **2011**, *49*, 3346–3354.
- (52) Akerlof, G. *J. Am. Chem. Soc.* **1932**, *54*, 4125–4139.
- (53) Derry, M. J.; Fielding, L. A.; Warren, N. J.; Mable, C. J.; Smith, A. J.; Mykhaylyk, O. O.; Armes, S. P. *Chem. Sci.* **2016**, *7*, 5078–5090.
- (54) Ihli, J.; Bots, P.; Kulak, A.; Benning, L. G.; Meldrum, F. C. *Adv. Funct. Mater.* **2013**, *23*, 1965–1973.
- (55) Wehrmeister, U.; Soldati, A. L.; Jacob, D. E.; Haeger, T.; Hofmeister, W. *J. Raman Spectrosc.* **2010**, *41*, 193–201.
- (56) Lovett, J. R.; Fielding, L. A.; Armes, S. P.; Buxton, R. *Adv. Funct. Mater.* **2014**, *24*, 1290–1299.
- (57) Jones, E.; Mykhaylyk, O.; Semsarilar, M.; Boerakker, M.; Wyman, P.; Armes, S. *Macromolecules* **2015**, *49*, 172–181.
- (58) Dey, R. E.; Zhong, X.; Youle, P. J.; Wang, Q. G.; Wimpenny, I.; Downes, S.; Hoyland, J. A.; Watts, D. C.; Gough, J. E.; Budd, P. M. *Macromolecules* **2016**, *49*, 2656–2662.